Solar Phys
DOI 10.1007/s11207-014-0591-x

Interaction Between Two CMEs During 14 – 15 February 2011 and Their Unusual Radio Signature

A. Shanmugaraju · S. Prasanna Subramanian · Bojan Vrsnak · M. Syed Ibrahim

Received: 30 October 2013 / Accepted: 2 August 2014

Abstract We report a detailed analysis of an interaction between two coronal mass ejections (CMEs) that were observed on 14 – 15 February 2011 and the corresponding radio enhancement, which was similar to the "CME cannibalism" reported by Gopalswamy *et al.* (*Astrophys. J.* **548**, L91, 2001). A primary CME, with a mean field-of-view velocity of 669 km s^{-1} in the *Solar and Heliospheric Observatory* (SOHO)/*Large Angle Spectrometric Coronagraph* (LASCO), was more than as twice as fast as the slow CME preceding it (326 km s^{-1}), which indicates that the two CMEs interacted. A radio-enhancement signature (in the frequency range 1 MHz – 400 kHz) due to the CME interaction was analyzed and interpreted using the CME data from LASCO and from the *Solar Terrestrial Relations Observatory* (STEREO) HI-1, radio data from *Wind*/*Radio and Plasma Wave Experiment* (WAVES), and employing known electron-density models and kinematic modeling. The following results are obtained: i) The CME interaction occurred around 05:00 – 10:00 UT in a height range 20 – 25 $R_\odot$. An unusual radio signature is observed during the time of interaction in the *Wind*/WAVES dynamic radio spectrum. ii) The enhancement duration shows that the interaction segment might be wider than 5 $R_\odot$. iii) The shock height estimated using density models for the radio enhancement region is 10 – 30 $R_\odot$. iv) Using kinematic modeling and assuming a completely inelastic collision, the decrease of kinetic energy based on speeds from LASCO data is determined to be 0.77×10^{23} J, and 3.67×10^{23} J if speeds from STEREO data are considered. vi) The acceleration, momentum, and force are found to be $a = -168$ m s^{-2}, $I = 6.1 \times 10^{18}$ kg m s^{-1}, and $F = 1.7 \times 10^{15}$ N, respectively, using STEREO data.

A. Shanmugaraju (✉) · M.S. Ibrahim
Arul Anandar College, Karumathur 625 514, Madurai District, India
e-mail: ashanmugaraju@gmail.com

S. Prasanna Subramanian
M.K. University College, Aundipatti, Theni District, India

B. Vrsnak
Faculty of Geodesy, Hvar Observatory, Zagreb, Croatia

Published online: 28 August 2014

Keywords Coronal mass ejections · Interacting coronal mass ejections · Type-II radio bursts

1. Introduction

Interactions of two coronal mass ejections (CMEs) have been investigated by Gopalswamy *et al.* (2001, 2002b, 2004), Liu, Luhmann, and Christian (2012), and Temmer *et al.* (2012) using white-light coronagraph images from *Solar and Heliospheric Observatory/Large Angle Spectrometric Coronagraph* (SOHO/LASCO) (Gopalswamy *et al.*, 2002b) and Type II spectra at long wavelengths from the *Radio and Plasma Wave Experiment* (WAVES) onboard the *Wind* spacecraft. Generally, interacting CMEs may contain two or more CMEs. The position-angle separation between the CMEs should be less than 90° and the flare locations should be close to each other. That is, the separation between the flare locations of the associated CMEs should be below 30°. The CME ejections from the same active region or nearby active regions can interact (Gopalswamy *et al.*, 2001). White-light coronagraph images provide optical evidence of interacting CMEs in the corona and interplanetary medium, and the radio dynamic spectrum reveals the enhancement/weakening of the radio intensity of CMEs. For example, Gopalswamy *et al.* (2001) suggested that the observed radio enhancement results from increased density in the upstream medium that reduces the Alfvén speed, thereby increasing the Mach number of shock. Gopalswamy *et al.* (2002a, 2004) also suggested that the radio enhancements in the Type II dynamic spectrum are only caused by the interaction. The current interpretation of interacting CMEs is that a slow preceding CME is being pushed from behind by the faster CME when they are both ejected from locations close to each other.

Since nonthermal radio emission is observed during interaction, Gopalswamy *et al.* (2001) suggested that proton accelerators are also good electron accelerators. Most interacting CMEs are associated with DH Type II radio bursts, and radio features are observed by the RAD-1 and RAD-2 receivers of the *Wind*/WAVES spacecraft. Gopalswamy *et al.* (2002b) investigated interacting CMEs associated with major solar energetic particle (SEP) events. There are also numerical-simulation studies of interaction between CMEs in the interplanetary medium (*e.g.* Lugaz, Manchester, and Gombosi, 2005). Recently, Martínez *et al.* (2012) and Temmer *et al.* (2012) have studied an interacting event on 01 August 2010 and suggested that the associated Type II burst radio emission is related to the CME interaction. The interacting CMEs during 30 July 2010 – 01 August 2010 and their shocks have been investigated by Liu, Luhmann, and Christian (2012), who reported changes in shock strength and global structure.

The primary CME (CME-B), which is characterized by a large width and high speed, was launched from the same active region as the slowly moving preceding CME (CME-A). All primary CMEs (CME-B) are found to be associated with major flares and decameter–hectometric (DH) Type II radio bursts (Prasanna Subramanian and Shanmugaraju, 2013; Shanmugaraju and Prasanna Subramanian, 2014). Ding *et al.* (2013) have analyzed a set of twin CMEs to identify whether a preceding-CMEs enhances the SEP intensity or not. They found that large SEP events tend to be twin CMEs.

There are several articles on the relationship between metric and DH Type II bursts associated with CMEs (Shanmugaraju *et al.*, 2003; Prakash *et al.*, 2009; Vasanth *et al.*, 2011). The relationship between solar flare, CME, and shock was studied by Vrsnak and Cliver (2008). Vrsnak *et al.* (2007) have studied the kinematics of CMEs. A study of interacting CMEs is rare. Maricic *et al.* (2014) studied the CME–CME interaction that occurred on 15 February 2011. They investigated the kinematics of interacting ICMEs and the Forbush

decrease for this event and found that the velocity of the CME-A increased and the speed of the CME-B decreased after the interaction. Interplanetary radio signatures of the interaction were not studied, however. The motivation for the study presented in this article is to extend the analysis performed by Maricic *et al.* (2014) and include the unusual radio feature observed that was caused by the interacting CMEs. The data for our study come from *Wind*/WAVES, SOHO/LASCO, and STEREO that were collected during 14 – 15 February 2011.

2. Data

White-light observations obtained by the LASCO coronagraph onboard SOHO were taken from cdaw.gsfc.nasa.gov (Yashiro *et al.*, 2004; Gopalswamy *et al.*, 2009). Even though several CMEs were launched prior to the primary CME (CME-B), we consider CME-A launched from the same active region at 18:24 UT on 14 February 2011 (Gopalswamy *et al.*, 2013a). Data for the radio spectrum in the metric wavelength range of radio bursts are provided by the Hiraiso Radio Spectrograph (HiRAS), Japan. Radio observations in the DH range obtained by the radio and plasma wave experiment onboard the *Wind*/WAVES spacecraft are listed in the online catalog. The flare data were taken from the X-ray flare website (www.ngdc.noaa.gov), which is maintained by the National Oceanic and Atmospheric Administration (NOAA). Table 1 gives the chronological order of events for the interacting event, such as flares associated with CME-A and CME-B, the source location, first appearance time in the LASCO-C2 and C3 field of view, onset time of the CMEs, details of metric and DH Type II bursts, and the height and time of CME interaction. The kinematics of the ICMEs from STEREO reported by Maricic *et al.* (2014) are also compared with the LASCO and *Wind*/WAVES data.

Table 1 Observational details of the interacting event during 14 – 15 February 2011. CME data are from SOHO/LASCO.

No.	Observation	Time	Distance
CME-A on 14 February 2011			
1	CME-A associated flare (M2.2) start time	17:20 UT	
2	Source location S20W04		
3	CME-A onset time	17:18 UT	
4	First C2 appearance	18:24 UT	2.85 $R_\odot$
5	First C3 appearance	20:06 UT	5.7 $R_\odot$
6	Final observed distance of CME-A		8.4 $R_\odot$
CME-B on 15 February 2011			
7	CME-B associated flare (X2.2) start time	01:44 UT	
8	Source location S20W12		
9	CME-B onset time	01:49 UT	
10	Appearance of metric Type IV radio burst associated with metric Type II radio burst from HiRAS spectrum.	≈01:50 UT	
11	Ending time of metric Type IV radio burst and DH Type II radio burst start	≈02:10 UT	
12	First C2 appearance	02:24 UT	2.43 $R_\odot$
13	First C3 appearance	03:06 UT	5.49 $R_\odot$
14	Interaction between the CME start	≈05:00 UT	≈20 $R_\odot$
15	"Cannibalism" radio signature at 1 MHz from RAD-1 receiver	≈05:00 UT	
16	Final observed distance of CME-B	06:54 UT	18.55 $R_\odot$

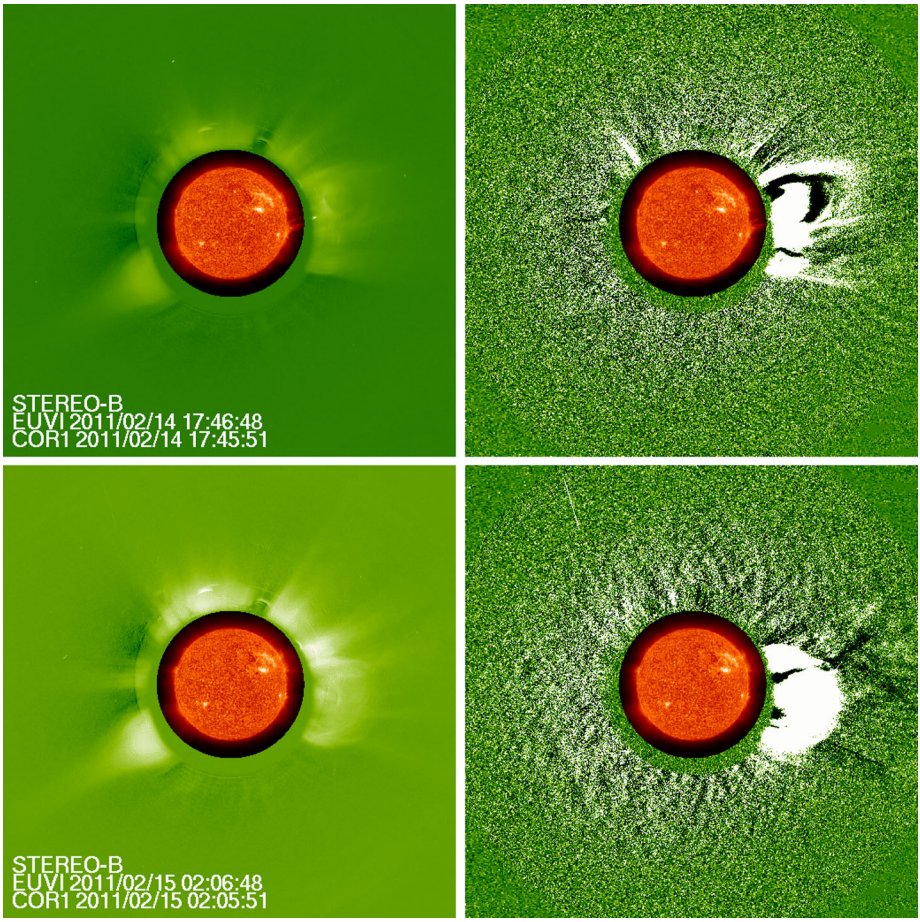

Figure 1 STEREO-B images on 14 February 2011 and 15 February 2011 of CME-A and CME-B. Left: EUVI/COR-1 images; right: running-difference COR-1 images.

3. Analysis and Results

3.1. CME Interaction and Associated Radio Signatures

First, an M-class flare was detected by the *Geostationary Operational Environmental Satellite* (GOES) at 17:20 UT on 14 February 2011. Then, a slow halo CME-A was observed by the LASCO-C2 coronagraph at 18:24 UT at a height of 2.85 $R_{\odot}$ with a linear propagation speed 326 $km\,s^{-1}$. The acceleration of the CME-A was reported as 4.6 $m\,s^{-2}$. At 1:44 UT, an intense X-class flare occurred at S20W12. Following this, at 2:24 UT a primary halo-CME (CME-B) with speed 669 $km\,s^{-1}$ was observed by SOHO/LASCO. This CME-B was reported to decelerate at $-18.3\ m\,s^{-2}$. CME-A and CME-B were also observed by the STEREO-A and B spacecraft. The *Extreme Ultraviolet Imager* (EUVI) and COR-1 images of these two CMEs are shown in Figure 1, which shows that two CMEs are ejected from the same active region (AR 11158).

CME-A and CME-B can also be identified as two individual features in the running-difference images of STEREO/HI-1 (Figure 2, left), but this is difficult in the CME–CME

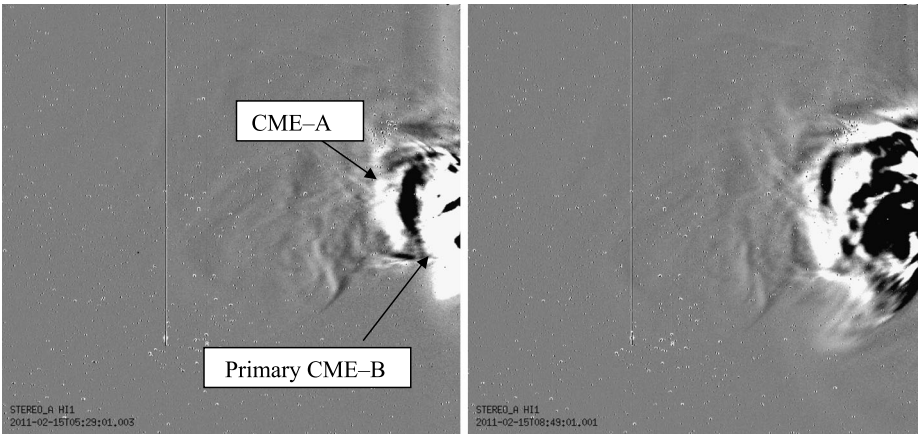

Figure 2 Running-difference images of STEREO-A/HI-1 showing CME-A and CME-B (left); CME–CME interaction around 08:50 UT (right).

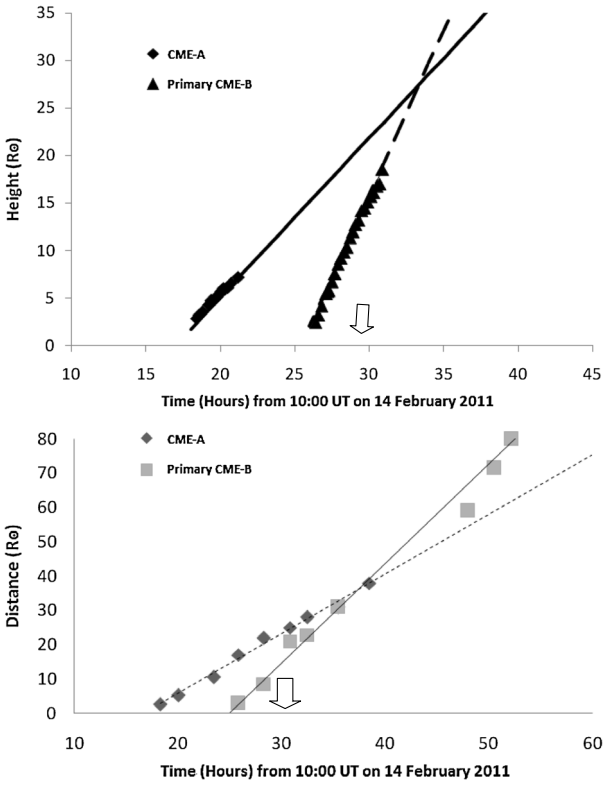

Figure 3 Height–time diagram showing the interaction of the two CMEs (top: SOHO/LASCO data, bottom: STEREO data). The time of the radio signature of the interaction is indicated by the arrow.

interaction image around 08:50 UT (Figure 2, right). Height–time diagrams of the two CMEs are shown together using the LASCO image in Figure 3 (top) and STEREO data in Figure 3 (bottom). The interaction of the two CMEs is clear in the height–time plot and coronagraph images. Since the SOHO/LASCO images are subject to projection effects, the CME inter-

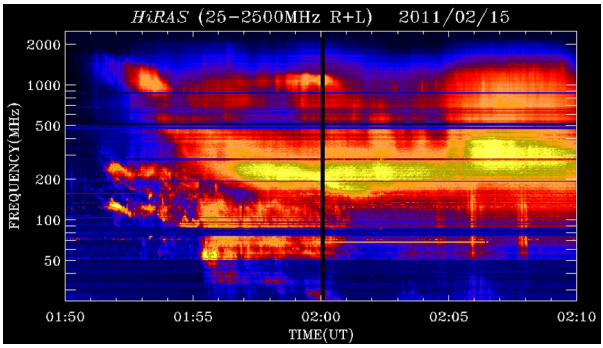

Figure 4 Hiraiso Radio Spectrograph (HiRAS) radio dynamic spectrum in the metric wavelength range, showing the Type II and Type IV radio bursts associated with CME-B. The metric Type II emission is observed from 01:50 UT to 02:00 UT below 300 MHz. The continuum broad-band metric Type-IV emission is observed during 01:50 UT to beyond 02:10 UT above 100 MHz (sunbase.nict.go.jp/solar/denpa/hirasDB/Events).

Figure 5 Dynamic spectrum showing the Type II burst in the range 14 000 – 400 kHz and interaction radio features around 05:00 UT (1000 – 400 kHz) recorded by the *Wind*/WAVES RAD-1 and RAD-2 receivers (www-lep.gsfc.nasa.gov/waves/bursts_2011.html).

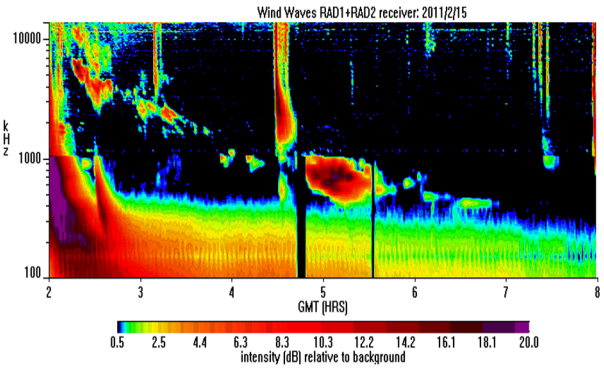

action can be clearly seen in the STEREO/HI-1 data in Figure 3 (bottom). The interaction occurred at around 30 – 35 hours after 14 February 2011, *i.e.* around 6 – 10 UT on 15 February 2011 at a height range of 20 – 25 $R_{\odot}$. These height–time data points are the leading-edge positions of the two CMEs.

The HiRAS radio dynamic spectrum in the metric frequency range showed Type II and Type IV radio bursts associated with the CME-B (Figure 4). Figure 4 reveals that the Type II and Type IV start at the same time: 01:51 UT. This starting time coincides with that reported by Maricic *et al.* (2014), who noted from STEREO/EUVI images that the CME-B on 15 February 2011 started at 01:50 UT. The continuation of the metric Type II is also seen in the DH range in the *Wind*/WAVES spectrum shown in Figure 5. The Type II shock was reported to form at a height of 1.21 $R_{\odot}$ based on the metric Type II data and STEREO/EUVI images (Gopalswamy *et al.*, 2013b). The metric Type II burst shows a strong intermittent tone with fundamental and harmonic features associated with the CME-B. The DH Type II burst also shows intermittent features from 02:00 – 07:00 UT in the frequency range of 14 MHz to 400 kHz. An unusual radio feature/enhancement is also observed in the *Wind*/WAVES dynamic spectrum around 05:00 UT. The X-ray flares associated with the CME-A and CME-B are shown in Figure 6.

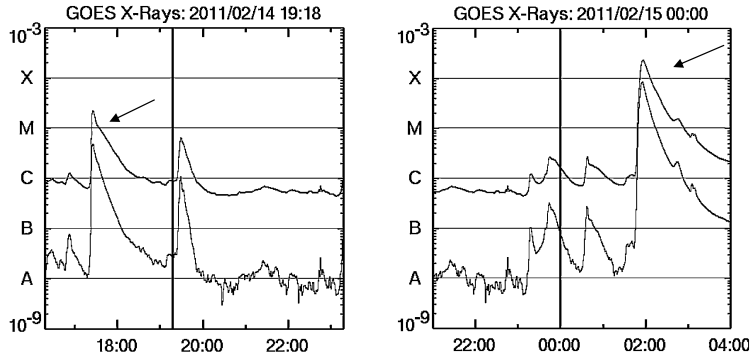

Figure 6 GOES X-ray flares associated with CME-A (left: M2.2 flare at 17:20 UT) and the primary CME-B (right: X2.2 flare at 01:44 UT) (cdaw.gsfc.nasa.gov/images/goes/xrs). The arrow indicates the corresponding flares. The vertical line denotes the time at the top of each plot.

3.2. Electron Density Models – Radio Signatures

From Figure 3, which shows the height–time data of the leading-edge positions of CMEs, the interaction height and time are estimated to be approximately 25 $R_\odot$ and 06:00 – 10:00 UT on 15 February 2011. Correspondingly, the *Wind*/WAVES Type II spectrum (Figure 5) shows an unusual radio signature similar to the radio enhancement due to CME cannibalism reported by Gopalswamy *et al.* (2001) during 04:45 – 05:45 UT in the frequency range 1000 – 400 kHz. Considering that the leading edge of the primary CME interacts with the trailing edge of CME-A, and taking into account the error in CME height measurements (Liu *et al.*, 2009; Liu, Luhmann, and Christian, 2012) in STEREO/HI-1 as well as the sudden deceleration of the CME-B after 03:00 UT, as mentioned in the next section, the difference in times of interaction derived from the height–time plots and radio enhancement are within the acceptable limits. As reported by Liu *et al.* (2009), the uncertainty in the measurement of the CME height in STEREO/HI-1 is estimated to be about ten pixels in the image (0.72 $R_\odot$). The height corresponding to this observational frequency range can be obtained using density models like those of Saito, Poland, and Munro (1977) and Leblanc, Dulk, and Bougeret (1998),

$$N_e = 1.36 \times 10^6 r^{-2.14} + 1.68 \times 10^8 r^{-6.13}, \quad (1)$$

$$N_e = 3.3 \times 10^5 r^{-2} + 4.1 \times 10^6 r^{-4} + 8.0 \times 10^7 r^{-6}, \quad (2)$$

because the emission frequency is related to electron density as

$$f_p \text{ (kHz)} = 9 N_e^{1/2}, \quad (3)$$

where N_e is the electron density expressed in cm^{-3}, r is the distance parameter in $R_\odot$, and f_p is the fundamental plasma frequency in kHz.

As seen from Figure 7, the source of the DH Type II burst observed in the frequency range 14 – 1 MHz is within 10 $R_\odot$ (as already suggested by Gopalswamy *et al.*, 2001). However, the height corresponding to the interaction radio feature is higher than 10 $R_\odot$. In addition, the entire frequency range of this radio enhancement (1000 – 400 kHz) can be emitted from a height range of 10 – 30 $R_\odot$, which is marked by a rectangle in Figure 7. When the frequency–height profile in this figure was extended to higher frequencies to confirm the origin of the

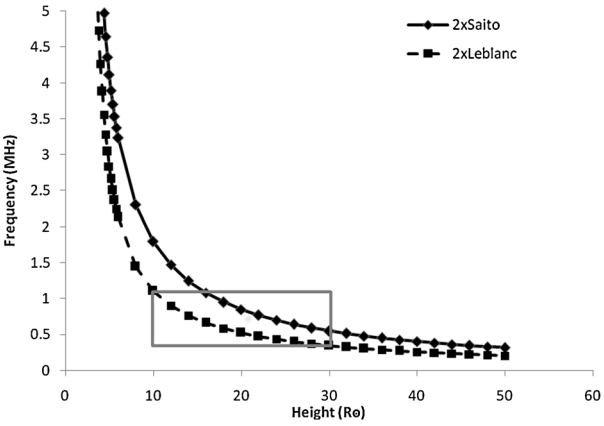

Figure 7 Frequency *versus* height derived from two electron-density models in the DH frequency range (Saito, Poland, and Munro, 1977, and Leblanc, Dulk, and Bougeret, 1998). A rectangle marks the region in which the radio features associated with the CME–CME interaction (frequency range: 1 – 0.4 MHz, height range 10 – 30 $R_\odot$) might have been generated.

metric Type II bursts that continue in the DH domain, the fundamental starting frequency (150 MHz) of the metric Type II burst leads to a height of ≈ 1.21 $R_\odot$ as determined by Gopalswamy *et al.* (2013b). In Figure 7, the y-axis is restricted in the DH range to show the interaction region.

3.3. Comparison of Observations Using STEREO and *Wind*/WAVES

Recently, Maricic *et al.* (2014) have analyzed the kinematics of CME–CME interaction during 13 – 15 February 2011 in detail. The results from their study can supplement our results to support the idea that the radio signatures seen around 05:00 UT are due to the interaction of CMEs. In their study, they found that the 14 February CME-A was chased by, and interacted with, the 15 February CME-B, and the speed of the two CMEs changed after the interaction. That is, the speed of the CME-A increased from 400 to 600 km s^{-1}, whereas the speed of the CME-B decreased to 600 km s^{-1} from its maximum speed of 1300 km s^{-1}. It was reported that the change of speed occurred around 28 $R_\odot$ during the time interval of an elapsed time of 32 – 37 hours from 00:00 UT on 14 February, *i.e.* 08:00 – 13:00 UT on 15 February.

The authors also reported that the strongest deceleration (-400 m s^{-2}) of CME-B was at an elapsed time of 27 hours (Figure 6 in Maricic *et al.*, 2014), *i.e.* around 03:00 UT on 15 February. Around this time, the front of the 15 February CME was at a distance of nearly 5 $R_\odot$. As reported in Gopalswamy *et al.* (2012), the CME-B traveled at a speed of ≈ 1000 km s^{-1} from 03:00 UT at height of 5 $R_\odot$, which means that it should reach ≈ 18 $R_\odot$ at 05:30 UT. This is quite consistent with the interaction height of $\approx 20 - 25$ $R_\odot$ and the radio enhancement around 05:30 UT. Furthermore, the results based on the density models shown in Figure 7 for the radio enhancement signatures (distance range of 10 – 35 $R_\odot$) are consistent with the finding of Maricic *et al.* (2014) that the interaction "signal" (probably the ICME-driven magnetosonic shock) traveled a distance range of 30 $R_\odot$.

In addition, according to Maricic *et al.* (2014), the collision was not fully symmetric, *i.e.* noninteracting segments moved faster than the interacting segments. This implies that the interacting segment faced a high-density region due to CME-A where the Alfvén speed might be low (Gopalswamy *et al.*, 2001; Vrsnak *et al.*, 2002), because $V_A \sim B/(N_e^{1/2})$, which led to the shock intensification. The duration of the radio-enhancement signature (one hour from 04:45 – 05:45 UT) can give some idea about the extent of the interacting CME segment (Gopalswamy *et al.*, 2001). If the shock associated with the CME-B travels

at a maximum speed of 1000 km s^{-1}, it can cross a distance of ≈ 5 R$_\odot$ in one hour. Hence, the extent of the CME interacting segment is not smaller than 5 R$_\odot$.

3.4. Kinematic Modeling of CME Interaction

The linear speed of a CME is listed in the CME catalog obtained from the height–time data from SOHO/LASCO. For interacting events, however, the velocity of the CME varies after interaction. We denote the velocities of CME-A and the primary CME-B before the interaction by u_1 and u_2, and by v_1 and v_2 the corresponding velocities after the interaction. Since both of the CMEs are propagating at slightly different central position angle (CPA), we consider this impact to be an oblique impact. We consider a 2D treatment of an interacting event along a common normal axis, where α and β define the direction (angles at which the preceding and primary CMEs travel with respect to the common normal axis of propagation of the CME-A and CME-B before the interaction). From Newton's experimental law of collision along a common normal axis $v_1 - v_2 = -e(u_1 - u_2)$, the loss of kinetic energy can be written in terms of initial velocities as

$$\Delta E = m_1 m_2 \big[1 - e^2\big][u_1 \cos\alpha - u_2 \cos\beta]^2 / \big[2(m_1 + m_2)\big], \tag{4}$$

where the symbols e, m_1, and m_2 refer to the elastic coefficient, the mass of the CME-A, and the mass of the CME-B. For a direct impact of CMEs that propagate along the same direction, $\cos\alpha = \cos\beta = 1$. Therefore the loss of kinetic energy is

$$\Delta E = m_1 m_2 \big[1 - e^2\big][u_1 - u_2]^2 / \big[2(m_1 + m_2)\big]. \tag{5}$$

If we assume the collision is completely inelastic [$e = 0$] then

$$\Delta E = m_1 m_2 [u_1 - u_2]^2 / \big[2(m_1 + m_2)\big]. \tag{6}$$

It is evident from LASCO data that the CME-A observed on 14 February 2011 was not as bright as the CME-B of 15 February. Hence, assuming the masses of CME-A and CME-B to be 10^{12} kg and 10^{13} kg, respectively, and using the velocity of CME-A and CME-B from LASCO data before impact as 326 km s^{-1} and 738 km s^{-1}, respectively, the loss of kinetic energy is estimated from Equation (5) as 0.77×10^{23} J. Similarly, using the velocity of the CME-A and CME-B from STEREO data (400 km s^{-1} and 1300 km s^{-1}), we find $\Delta E = 3.67 \times 10^{23}$ J, which is only slightly higher than that obtained using LASCO speeds.

Using the kinetic energies of the two CMEs before and after the interaction [$\frac{1}{2}m_1u_1^2 + \frac{1}{2}m_2u_2^2 = \frac{1}{2}m_1v_1^2 + \frac{1}{2}m_2v_2^2$] the loss of kinetic energy is calculated as 6.55×10^{24} J (for the speeds from STEREO data). Note that this value is one order of magnitude greater than the values obtained above. Moreover, the value might be the maximum limit because we show below (Figure 8) that for a completely inelastic collision [$e = 0$] the loss of kinetic energy attains a maximum value. From Newton's experimental law of collision along a common normal axis [$v_1 - v_2 = -e(u_1 - u_2)$], the coefficient of elastic collision must be zero for the speeds measured using STEREO (Maricic *et al.* (2014), due to the same speed of CME-A and CME-B ($v_1 = v_2 = 600$ km s^{-1}) after the interaction.

The momentum transferred from CME-B to CME-A during the interaction period at the overlapping angle [δ: width of overlap between central position angles of CME-A and CME-B, Gopalswamy *et al.* (2002b)] is defined as

$$I = m_2(v_2 - u_2)\cos\delta. \tag{7}$$

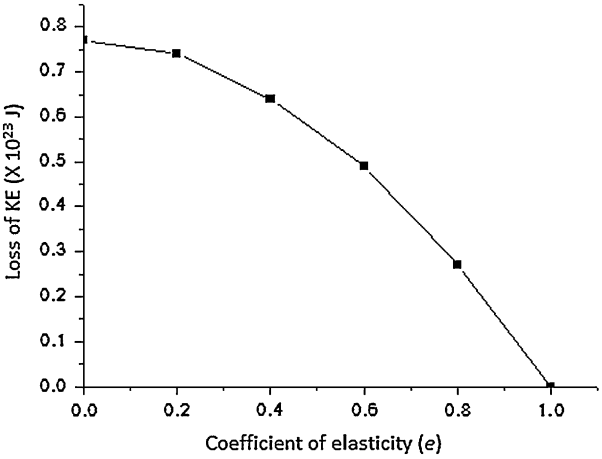

Figure 8 Loss of the kinetic energy *versus* coefficient of elasticity plotted for the CME speeds measured using the LASCO data.

Assuming an overlapping angle $\delta = 30^{\circ}$, the impulse is calculated as 1.03×10^{18} kg m s^{-1} (using speeds from LASCO data and $m_2 = 10^{13}$ kg). From the radio features of the *Wind*/WAVES dynamic spectra, the radio-enhancement-signature duration may be taken as the interaction duration ($\Delta t =$ one hour). This interaction duration can be used to estimate the force as

$$F = m_2(v_2 - u_2)\cos\delta/\Delta t. \tag{8}$$

Using the speeds from STEREO data [$u_2 = 1300$ km s^{-1}, $v_2 = 600$ km s^{-1}], the momentum is $I = 6.06 \times 10^{18}$ kg m s^{-1} and the force $F = 1.68 \times 10^{15}$ N, which leads to a deceleration of -168 m s^{-2}. Maricic *et al.* (2014) reported a peak deceleration value of -400 m s^{-2} for CME-B after the interaction. To obtain this value, the force would need to be 4×10^{15} N and hence the interaction duration would need to be $\Delta t = 25$ minutes instead of the 60 minutes as we assumed above. A peak deceleration of 400 m s^{-2} means that the mean deceleration was lower by about 200 m s^{-2}. This argument agrees with the deceleration of -168 m s^{-2} estimated above.

Recently, Temmer *et al.* (2012) suggested that the CME interaction might be neither completely inelastic nor completely elastic. Hence, we obtained the loss of kinetic energy from Equation (5) for intermediate values of the elastic coefficient [e] as shown in Figure 8. For a completely inelastic collision [$e = 0$] the loss of kinetic energy attains its maximum value. For a value between 0.1 and 0.9, called partially elastic, the loss of kinetic energy decreases gradually. The elastic coefficient $e = 1$ represents the completely elastic type of collision.

4. Summary and Conclusion

An interaction between two CMEs observed during 14 – 15 February 2011 and the corresponding radio enhancement were analyzed in detail in this article using multiwavelength data from SOHO/LASCO, STEREO/HI-1, and *Wind*/WAVES. The interacting CMEs produced a shock strengthening similar to that in "CME cannibalism" reported by Gopalswamy *et al.* (2001) from *Wind*/WAVES decameter–hectometric observations. A primary CME (CME-B) observed by SOHO/LASCO with a linear velocity of 669 km s^{-1} that was ejected around 02:00 UT on 15 February 2011 interacted with a slow CME (CME-A) (326 km s^{-1})

ejected around 18:00 UT on 14 February 2011. Associated with the CME interaction, a radio enhancement signature was observed in the frequency range 1 MHz – 400 kHz.

First, these data of the interacting event were analyzed using electron-density models (Saito, Poland, and Munro, 1977, and Leblanc, Dulk, and Bougeret, 1998). Then, the interacting event was treated using kinematic modeling to estimate various kinematic parameters. The results obtained in the above analysis are the following:

i) The CME interaction occurred around 05:00 – 10:00 UT on 15 February 2011 at a height of about 25 $R_{\odot}$. An unusual radio signature is observed during the time of interaction in the *Wind*/WAVES decameter–hectometric radio spectrum.
ii) The enhancement duration showed that the interaction segment could be 5 $R_{\odot}$ wide.
iii) The shock height estimated using the density models for the radio enhancement is 10 – 30 $R_{\odot}$.
iv) Using kinematic modeling and assuming completely inelastic collision, the loss of kinetic energy was determined to be 0.77×10^{23} J using speeds from LASCO data; using speeds from STEREO data, one finds 3.67×10^{23} J.
v) The momentum $[I]$, force $[F]$, and acceleration $[a]$ obtained for the STEREO data are equal to 6.06×10^{18} kg m s^{-1}, 1.68×10^{15} N, and -168 m s^{-2}, respectively.

Acknowledgements The grant No. 42–845/2013 (SR) to AS from the University Grants Commission, Govt. of India is kindly acknowledged. We would like to thank P.K. Manoharan (Radio Astronomy Centre, NCRA-TIFR, Ooty, India) for constructive discussions. We thank the referee for giving valuable points to improve this work. We also acknowledge the data from LASCO, GOES, STEREO, *Wind*/WAVES, and HiRAS and thank the respective teams for their open data policy.

References

Ding, L., Jiang, Y., Zhao, L., Li, G.: 2013, *Astrophys. J. Lett.* **763**, 30.
Gopalswamy, N., Yashiro, S., Kaiser, M.L., Howard, R.A., Bougeret, J.L.: 2001, *Astrophys. J. Lett.* **548**, L91.
Gopalswamy, N., Yashiro, S., Kaiser, M.L., Howard, R.A., Bougeret, J.L.: 2002a, *Geophys. Res. Lett.* **29**(8), 1265. DOI.
Gopalswamy, N., Yashiro, S., Michałek, G., Kaiser, M.L., Howard, R.A., Reames, D.V., Leske, R., Von Rosenvinge, T.: 2002b, *Astrophys. J. Lett.* **572**, L103.
Gopalswamy, N., Yashiro, S., Krucker, S., Stenborg, G., Howard, R.A.: 2004, *J. Geophys. Res.* **109**(A12), A12105.
Gopalswamy, N., Yashiro, S., Michalek, G., Stenborg, G., Vourlidas, A., Freeland, S., Howard, R.: 2009, *Earth Moon Planets* **104**, 295.
Gopalswamy, N., Makela, P., Yashiro, S., Davila, J.M.: 2012, *Sun Geosph.* **7**, 7.
Gopalswamy, N., Makela, P., Xie, H., Yashiro, S.: 2013a, *Space Weather* **11**, 661.
Gopalswamy, N., Xie, H., Makela, P., Yashiro, S., Akiyama, S., Uddin, W., Srivatsava, A.K., *et al.*: 2013b, *Adv. Space Res.* **51**, 1981.
Leblanc, Y., Dulk, G.A., Bougeret, J.-L.: 1998, *Solar Phys.* **183**, 165. ADS. DOI.
Liu, Y., Luhmann, J.G., Christian, M.: 2012, *Astrophys. J. Lett.* **746**(2), L15.
Liu, Y., Luhmann, J.G., Bale, S.D., Lin, R.P.: 2009, *Astrophys. J. Lett.* **691**, L151.
Lugaz, N., Manchester, W.B., Gombosi, T.I.: 2005, *Astrophys. J.* **634**, 651.
Maricic, D., Vrsnak, B., Dumbovic, M., Zic, T., Rosa, D., Hezina, D., *et al.*: 2014, *Solar Phys.* **289**, 351.
Martínez, O., Juan, C., Raftery, C.L., Bain, H.M., Liu, Y., Krupar, V., Bale, S., Krucker, S.: 2012, *Astrophys. J.* **748**, 66.
Prakash, O., Umapathy, S., Shanmugaraju, A., Vršnak, B.: 2009, *Solar Phys.* **258**, 105. ADS. DOI.
Prasanna Subramanian, S., Shanmugaraju, A.: 2013, *Astrophys. Space Sci.* **344**(2), 305.
Saito, K., Poland, A.I., Munro, R.H.: 1977, *Solar Phys.* **55**, 121. ADS. DOI.
Shanmugaraju, A., Moon, Y.J., Dryer, M., Umapathy, S.: 2003, *Solar Phys.* **217**, 301. ADS. DOI.
Shanmugaraju, A., Prasanna Subramanian, S.: 2014, *Astrophys. Space Sci.* **352**, 385.
Temmer, M., Vrsnak, B., Rollett, T., Bein, B., de Koning, C.A., Liu, Y., Bosman, E., *et al.*: 2012, *Astrophys. J.* **749**, 57.

Vasanth, V., Umapathy, S., Vrsnak, B., Mahalakshmi, M.: 2011, *Solar Phys.* **273**, 143. ADS. DOI.
Vrsnak, B., Cliver, E.W.: 2008, *Solar Phys.* **253**, 215. ADS. DOI.
Vrsnak, B., Magdalenić, J., Aurass, H., Mann, G.: 2002, *Astron. Astrophys.* **396**, 673.
Vrsnak, B., Maricic, D., Stanger, A.L., Veronig, A.M., Temmer, M., Rosa, D.: 2007, *Solar Phys.* **241**, 85.
Yashiro, S., Gopalswamy, N., Michałek, G., St. Cyr, O.C., Plunkett, S.P., Rich, N.B., Howard, R.A.: 2004, *J. Geophys. Res.* **109**, 7105.